Decay Dynamics of 3-methyl-3-pentene-2-one from the light absorbing S2(ππ*) state - Resonance Raman Spectroscopy and CASSCF Study

7 AUTHORS, INCLUDING:

Xuming Zheng
Zhejiang Sci-Tech University
109 PUBLICATIONS **1,259** CITATIONS

SEE PROFILE

Wei-Hai Fang
Beijing Normal University
233 PUBLICATIONS **4,472** CITATIONS

SEE PROFILE

Decay Dynamics of 3-methyl-3-pentene-2-one from the light absorbing $S_2(\pi\pi^*)$ state - Resonance Raman Spectroscopy and CASSCF Study

Zhu-Bing Xu,[a] Sheng Pan,[a] Yi Yang,[a] Jia-Dan Xue,[a] Xuming Zheng,[a,b,c]* Bin-Bin Xie[d] and Wei-Hai Fang[d]*

The photophysics of 3-methyl-3-pentene-2-one (3M3P2O) after excitation to the $S_2(\pi\pi^*)$ electronic state were studied using the resonance Raman spectroscopy and complete active space self-consistent field (CASSCF) method calculations. The A-band resonance Raman spectra were obtained in cyclohexane, acetonitrile, and methanol with excitation wavelengths in resonance with the first intense absorption band to probe the structural dynamics of 3M3P2O. The B3LYP-TD/6-31++G(d, p) computation was carried out to determine the relative A-band resonance Raman intensities of the fundamental modes, and the result was used to reproduce the corresponding fundamental band intensities of the 223.1 nm resonance Raman spectrum and thus to examine whether the vibronic-coupling existed in Franck-Condon region or not. CASSCF calculations were carried out to determine the minimal singlet excitation energies of $S_{1,\ FC}$, $S_{1,min}$ $(n\pi^*)$, $S_{2,\ FC}$, $S_{2,min}$ $(\pi\pi^*)$, the transition energies of the conical intersection points S_n/S_π, S_n/S_0, and the optimized excited state geometries as well as the geometry structures of the conical intersection points. The A-band short-time structural dynamics and the corresponding decay dynamics of 3M3P2O were obtained by the analysis of the resonance Raman intensity pattern and CASSCF computations. It was revealed that the initial structural dynamics of 3M3P2O was towards the simultaneous $C_3=C_4$ and $C_2=O_7$ bond elongation, with the $C_3=C_4$ bond length lengthening greater at the very beginning, whereas the $C_2=O_7$ bond length changing greater at the later evolution time before reaching the $CI(S_2/S_1)$ conical intersection point. The decay dynamics from $S_2(\pi\pi^*)$ to $S_1(n\pi^*)$ via $S_2(\pi\pi^*)/S_1(n\pi^*)$ in singlet realm and from $S_1(n\pi^*)$ to $T_1(n\pi^*)$ via $ISC[S_1(n\pi^*)/T_2(\pi\pi^*)/T_1(n\pi^*)]$ in triplet realm are proposed. Copyright © 2014 John Wiley & Sons, Ltd.

Additional supporting information may be found in the online version of this article at the publisher's web site.

Introduction

The photochemistry and photophysics of α,β-enones has been the subject of many experimental and theoretical studies over the past half century. The lowest singlet and triplet excited states (S_1 and T_1) of the simplest α,β-enones, acrolein, were assigned by Walsh as the $n \rightarrow \pi^*$ transitions, whereas the S_2 state the $\pi \rightarrow \pi^*$ transition on the bases of electronic spectroscopic observation.[1] Becker et al. found that photoexcitation of acrolein into $S_1(n\pi^*)$ state resulted in the fluorescence with low yield because of fast internal conversion to S_0 or intersystem crossing to the $T_1(^3\pi\pi^*)$ dark state that lies very close to $S_1(n\pi^*)$.[2] Photolysis of acrolein in the $S_1(n\pi^*)$ state (at 313 nm) in the gas phase resulted in the photoproducts CO and CH_2CH_2, as well as the transient species CH_2—CH and HCO,[3] whereas the laser photo-fragmentation of acrolein in a supersonic molecular beam in the $S_2(\pi\pi^*)$ state (at 193 nm) formed the primary species CH_2CH and HCO, which suggested that the dissociation probably proceeded on the $S_1(n\pi^*)$ potential energy surface via the $S_2(\pi\pi^*)$ to $S_1(n\pi^*)$ internal conversion.[4] Comparative studies indicated that the photoisomerization of acrolein to methylketene took place prior to the dissociation process: CH_2=CHCHO → CH_3CHCO → $CH_3CH + CO$.[5,6] The molecular beam time-of-flight experiment revealed three distinct dissociation

pathways for the 193 nm photodissociation of acrolein: the molecular channel to $CH_2CH_2 + CO$, the radical channel to $CH_2CH + HCO$, and the hydrogen channel to $CH_2CHCO + H$.[7] Arendt et al. pointed out that the photodissociation of acrolein, acrylic acid, and acryloyl chloride (all have a C=C—C=O backbone) does not proceed through a single, direct dissociation mechanism, but rather via a predissociative way leading to the final dissociation

* *Correspondence to: Xuming Zheng, Department of Chemistry, Zhejiang Sci-Tech University, Hangzhou 310018, China.*
E-mail: zxm@zstu.edu.cn

** *Correspondence to: Wei-Hai Fang, Department of Chemistry, Beijing Normal University, Beijing, 100875, China.*
E-mail: fangwh@bnu.edu.cn

a *Department of Chemistry, Zhejiang Sci-Tech University, Hangzhou 310018, China*

b *Key Laboratory of Advanced Textiles Materials and Manufacture Technology of the Ministry of Education, Zhejiang Sci-Tech University, Hangzhou 310018, China*

c *Engineering Research Center for Eco-dyeing and Finishing of Textiles of the Ministry of Education, Zhejiang Sci-Tech University, Hangzhou 310018, China*

d *Department of Chemistry, Beijing Normal University, Beijing 100875, China*

channels,[8] as was similarly predicted from the experimental observation of a strong participation of the internal degrees of freedom.[7] The triplet lifetimes of several α,β-enones have been determined by Bonneau and Schuster et al.[9] to be ranged from 8 ns for methyl vinyl ketone and 11 ns for cycloheptenone[9] up to 185 ns for cyclopentenone.[10] The short triplet lifetime of methyl vinyl ketone has been attributed to facile intersystem crossing near the twisted minimum on the $T_1(^3\pi\pi^*)$ potential energy surface to a maximum on the ground-state (S_0) surface.[11]

The photochemistry and photophysics of acrolein have been studied using CASSCF/6-31G* calculations.[12] Two different photochemically active relaxation paths starting from a planar S_1 ($n\pi^*$) state minimum were revealed. The first one involves a radiationless decay to the triplet manifold via $S_1(n\pi^*)/T_1(\pi\pi^*)$ intersystem crossing, leading to the production of a short-lived $T_1(^3n\pi^*)$ twisted intermediate. This intermediate then decays, via a second intersystem crossing, to the ground state, leading to isomerization of the acrolein double-bond. The second one involves the singlet manifold only. Relaxation to S_0 occurs in a single decay channel via a $S_1(n\pi^*)/S_0$ conical intersection. The existence of a $T_1(^3n\pi^*)$ intermediate is supported by the observation of a 280-310-nm transient absorption in both acyclic and cyclic a, β-enones. Ab initio molecular orbital methods have been used to investigate the ground-state and excited-state potential energy surfaces (PESs) of acrolein.[13] The potential energy profiles, governing the dissociation of CH_2CHCHO to $CH_3CH + CO$, $CH_2CH + CHO$, and $CH_2CHCO + H$ in the ground state as well as in the excited singlet and triplet states, have been determined using different ab initio quantum mechanical methods. The most probable mechanism leading to different products is characterized on the basis of the obtained potential energy profiles and their crossing points. Also, the geometric and electronic structures of some low-lying electronic states of acrolein, methylketene, methylcarbene, and the CH_2CHCO radical are determined by the CASSCF computations. The ground and triplet excited states of cycloheptenone, cyclohexenone, and cyclopentenone have been studied using CASSCF calculations.[14] The difference in energy (ΔE) between the twisted $T_1(^3\pi\pi^*)$ minimum and $T_1(^3\pi\pi^*)/S_0$ intersection for three molecules increases as the flexibility of the ring decreases. A strong positive correlation between ΔE and the natural logarithm of the experimentally determined triplet lifetimes (lnτ) is found, suggesting that ΔE predominantly determines the relative radiationless decay rates of T_1.

Femtosecond time-resolved photoelectron spectroscopy and high-level theoretical calculations were used to study the effects of methyl substitution on the electronic dynamics of the α,β-enones: acrolein (2-propenal), crotonaldehyde (2-butenal), methylvinylketone (3-buten-2 -one), and methacrolein (2-methyl-2-propenal).[15] Following excitation to the $S_2(\pi\pi^*)$ state at 209 and 200 nm, the molecules move rapidly away from the Franck-Condon region (FC), reaching a conical intersection promoting relaxation to the $S_1(n\pi^*)$ state. Once on the S_1 surface, the trajectories access another conical intersection, leading them to the ground state. Only small variations between molecules are seen in their S_2 decay times. However, the position of methyl group substitution greatly affects the relaxation rate from the S_1 surface and the branching ratios to the products.

Up to now, the structural dynamics of α,β-enones in FC has not been studied. We report in this paper the resonance Raman spectroscopic and CASSCF calculation study of 3-methyl-3-pentene-2-one (3M3P2O) to better understand the excited state structures and decay dynamics of α,β-enones.

Experiments and computational methods

The FT (Fourier transform)-Raman and FT-IR spectra were obtained using FT-Raman (Thermo Nicolet 960, Thermo Fisher Nicolet, USA) and FT-IR (Thermo Nicolet avatar 370, Thermo Fisher Nicolet, USA) spectrometers with 2 cm^{-1} resolution. The ultraviolet (UV) absorption spectra and the FT-Raman spectra of 3M3P2O were measured using UV/visible spectrometer (UV-2501PC, Shimadzu, Japan). The experimental apparatus used to acquire the resonance Raman spectra of 3M3P2O have been described previously[16,17], so only a short description will be provided here. The harmonics of a nanosecond Nd:YAG laser and their hydrogen Raman shifted laser lines were utilized to generate the 208.8, 217.8, 223.1, 239.5, and 252.7 nm excitation wavelengths required for the resonance Raman experiments. The excitation laser beam used a ~100 μJ pulse energy loosely focused to a ~1.0 mm diameter spot size onto a flowing liquid stream of sample to excite the sample. A backscattering geometry was employed to excite a flowing liquid jet of sample and collect the Raman scattered light with reflective optics that imaged the light through a polarizer and entrance slit of a 0.5 m spectrograph. The grating of the spectrograph dispersed the Raman scattering light onto a liquid nitrogen-cooled charge coupled device detector. The Raman signal was collected for about 90–120 s before being read out to an interfaced PC computer and 30–40 of these readouts were added together to get the resonance Raman spectrum. The Raman shifts of the resonance Raman spectra were calibrated with the known vibrational frequencies of the cyclohexane solvent (99.9%, spectroscopic grade, Honeywell) Raman bands and the solvent Raman bands were then subtracted from the resonance Raman spectra by utilizing an appropriately scaled solvent spectrum. Sections of the resonance Raman spectra were fit to a baseline plus a sum of Lorentzian bands to determine the integrated areas of the Raman bands of interest. The solution phase samples used concentrations of approximately ~6.0 mmol·L^{-1} 3M3P2O (>95.0%, Tokyo Chemical industry Co. Ltd) in acetonitrile (99.9%, spectroscopic grade, TEDIA), in methanol (99.5%, spectroscopic grade, Tianjin Yongda chemical Reagent company limited) and in cyclohexane (99.9%, spectroscopic grade, TEDIA).

The complete geometry optimization and vibrational frequency computations were carried out for ground state 3M3P2O using the B3LYP/6−31+G(d) level of theory and under C_s symmetry constrain. The vertical transition energy for $S_0 \rightarrow S_n$ were estimated at B3LYP-TD/6−31+G(d) level. All the discrete Fourier transform calculations were carried out using the Gaussian 03 program.[18] The complete active space self-consistent field (CASSCF) theory was used to study the excited state decay mechanism of 3M3P2O. The conical intersection and intersystem crossing points between two electronic excited states were computed at CASSCF (6,5)/6−31G(d) level of theory. An active space with six electrons in five orbitals is referred to as CASSCF(6,5) hereafter.

Results and discussion

UV spectra and vertical electronic transitions

Figure 1 shows the UV spectra of 3M3P2O in cyclohexane, acetonitrile, and methanol with the five excitation wavelengths used for the resonance Raman experiments indicated earlier the curves. Table 1 lists the experimental and B3LYP-TD/6−31+G(d) computed singlet electronic transition energies of 3M3P2O. The
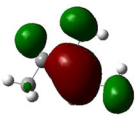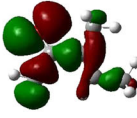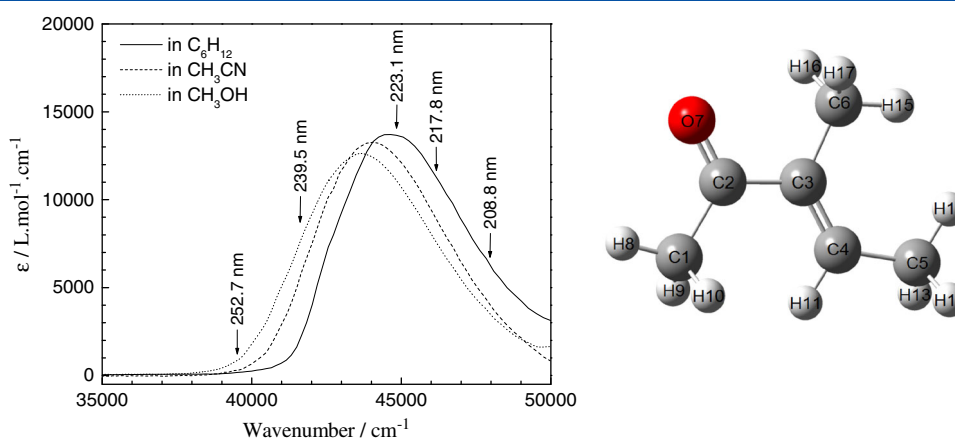
Figure 1. (Left) Ultraviolet spectra of 3M3P2O in cyclohexane (solid line), acetonitrile (dash line), and methanol (dot line). (Right) The B3LYP-TD/6−31 + G(d) optimized geometry structure of 3M3P2O.

Table 1. Experimental and B3LYP-TD/6−31 + G(d) computed singlet electronic transition energies of 3M3P2O at the optimized ground-state geometry and molecular orbitals associated with the electronic transitions
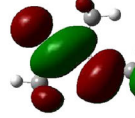
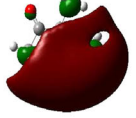| State	Orbitals	Character	Transition energy/nm (eV)		Oscillator strength (f)	
			Calc.	Expt.	Calc.	Expt.
$S_1(A'')$	$27 \rightarrow 28$ (0.70)	$n_H \rightarrow \pi_L^*$	330 (3.76)		0.0003	
$S_2(A')$	$26 \rightarrow 28$ (0.69)	$\pi_{H-1} \rightarrow \pi_L^*$	225 (5.52)	224.8	0.3313	0.3221
$S_3(A')$	$27 \rightarrow 29(0.69)/27 \rightarrow 31(0.11)$	$n \rightarrow Ryd_{L+1}^*/n \rightarrow Ryd_{L+3}^*$	203 (6.11)		0.0129	

Orbital 26 / π_{H-1} Orbital 27 / n   Orbital 28 / π_L^* Orbital 29 / Ryd_1^*

intense experimental band at 225 nm (A-band) has the oscillator strength $f = 0.3221$. This is in a good agreement with the calculated bright $S_2(\pi\pi^*)$ state at 225 with $f = 0.3313$. Thus, the A-band absorption is assigned as the $\pi_{H-1} \rightarrow \pi_L^*$ transition on the basis of Table 1. The calculated $S_1(n_H\pi_L^*)$ state located at 330 nm is a dark state and is assigned as the $n_H \rightarrow \pi_L^*$ transition.

The broad and featureless band shape, the large molar coefficient, and the full-width half-maximum for the A-band absorption of 3M3P2O in cyclohexane are basically similar to those in acetonitrile and methanol. This suggests that solvent-induced inhomogeneous broadening may not be as important as lifetime induced pure dephasing in contributing to the bandwidth broadening of the spectrum. The λ_{max} is shifted from 224.8 nm in cyclohexane to 229.0 nm in methanol, and this indicates that polarity and/or hydrogen bonding of solvent affect slightly the transition energy of the A-band absorption. It is clearly shown that the 208.8, 217.8, 223.1, 239.5, and 252.7 nm excitation wavelengths used in the resonance Raman experiments should mostly be on resonance with the A-band absorption.

The vibrational spectra and assignment

Figure S1 (Supporting Information) presents the experimental FT-Raman spectra of 3M3P2O in cyclohexane, acetonitrile and methanol and their comparison to that in neat liquid. Table 2

summarizes the experimental and B3LYP/6-31+G(d) computed vibrational frequencies and their tentative assignments. The results indicate that the frequency shifts for most of the vibrational bands are within 2 cm^{-1} in 0–1650 cm^{-1} region. Largest frequency shifts upon solvation appears in 1666 cm^{-1} band, which is 1672 cm^{-1} in cyclohexane to 1666 cm^{-1} in acetonitrile. Comparison of the experimental FT-Raman and FT-IR spectra with the B3LYP-TD/6−31 + G(d) computed vibrational spectrum of 3M3P2O indicates that there is a good agreement between the experimental frequencies and the calculated ones.

The correlation of the experimental FT-Raman spectrum of 3M3P2O in neat liquid to the calculated one is carried out. In 0–1000 cm^{-1} region, the experimental FT-Raman spectrum displays about ten Raman bands at 197, 233, 407, 486, 586, 602, 717, 825, 910, and 960 cm^{-1}. They correlate well with the calculated Raman bands at 202, 237, 406, 482, 586, 612, 714, 855, 908, and 960 cm^{-1}, respectively. Thus, the bands at 233, 407, 486, 586, 717, 910, and 960 cm^{-1} are respectively assigned as v_{28}, v_{26}, v_{25}, v_{24}, v_{23}, v_{22}, and v_{21} in A' irreducible representation, whereas the remaining three bands at 197, 602, and 825 cm^{-1} are respectively assigned as v_{41}, v_{39}, and v_{38} in A" irreducible representation. Similarly, in 1000–1300 cm^{-1} region, the experimental Raman bands at 1024, 1082, 1132, and 1271 cm^{-1} can correlate well with the calculated ones at 1024, 1093, 1142, and 1279 cm^{-1} in A' irreducible representation,

Table 2. B3LYP/6−31 + G(d) computed and experimentally observed vibrational frequencies and assignments of 3M3P2O

mode	Computed a	Computed b	FT-Raman	FT-IR	R-Raman c	Assignment, PED (%)
A′ ν_1	3176	3107	3062(w)	3057		ν C4H11 (52) + ν C5H12 (25)
ν_2	3160	3091	3016(w)	2999		ν C1H8(44) + sym ν H9C1H10(38)
ν_3	3155	3086				ν C6H15 (45) + ν C5H12 (33)
ν_4	3141	3073				ν C6H15 (41) + ν C5H12 (44)
ν_5	3060	2994	2970(vw)	2974		sym ν C6-3H (94)
ν_6	3054	2988	2925(Vs)	2929		sym ν C1-3H (99)
ν_7	3033	2967	2858(m)	2860		sym ν C5-3H (88)
ν_8	1736	1704	1666(vs)	1666	1678	ν C2O7(92)
ν_9	1709	1678	1645(vs)	1645	1643	ν C3C4(86)
ν_{10}	1513	1487	1444(m)	1435	1436	δ C6-3H (44) + δ C5-3H (44)
ν_{11}	1504	1479				δ C6-3H (41) + δ C5-3H (42)
ν_{12}	1497	1472				δ C1-3H (73)
ν_{13}	1447	1423	1392(w)	1392		C6-3H umbrella(67) + δ C4H11 (17)
ν_{14}	1437	1413	1381(w)	1385		C5-3H umbrella(58) + δ C4H11 (37)
ν_{15}	1413	1390	1360(w)			C1-3H umbrella(43) + C6-3H umbrella(16) + δ C4H11(20)
ν_{16}	1393	1370	1340(w)	1338	1360	C1-3H umbrella(34) + δ C4H11(36)
ν_{17}	1299	1279	1271(m)	1271		ν C2C3(30) + δ C1H8 (20) + δ C4H11(26)
ν_{18}	1158	1142	1132(w)	1132	1130	δ C5H12 (34) + δ C1H8(36) + δ C6H15 (14)
ν_{19}	1108	1093	1082(w)	1082	1083	δ C6-3H (65) + δ C5H12 (14) + ν C3C4(15)
ν_{20}	1037	1024	1024(m)	1022		δ C4H11 (20) + δ C1-3H(30) + δ C5-3H (38)
ν_{21}	972	960	960(m)	958	954	δ C5-3H (31) + δ C1-3H (44)
ν_{22}	919	908	910(vw)	914		δ C6-3H (43) + ν C1C2(25) + ν C4C5(20)
ν_{23}	719	714	717(s)	715		δ C5-3H (33) + C4C3C6 scissor(45)
ν_{24}	587	586	586(m)	584	593	δC1H8 (21) + δC2O7(17) + δC6H15 (25) + δC5H12 (36)
ν_{25}	481	482	486(m)	486	487	C2C3C4 scissor(65)
ν_{26}	403	406	407(m)		407	δ C1C2 (34) + δ C4C5(35)
ν_{27}	333	338				δ C3C6 (47) + δ C4C5(23)
ν_{28}	229	237	233(w)			δ C3C4C5 (52) + δ C1C2C3 (39)
A″ ν_{29}	3113	3045	3006(w)			asym ν H9C1H10 (92)
ν_{30}	3108	3041				asym ν H16C6H17 (87)
ν_{31}	3072	3005	2973(vw)			asym ν H13C5H14 (90)
ν_{32}	1507	1481				δ C1-3H (51)
ν_{33}	1505	1480				δ C5-3H (45) + δ C1-3H (34)
ν_{34}	1500	1475				δ C6-3H (64)
ν_{35}	1079	1065	1076(w)			δ C6-3H (53) + ρ_r H9C1H10 (19)
ν_{36}	1072	1058				ρ_r H13C5H14(64) + ρ_w C4H11 (35)
ν_{37}	1047	1034				ρ_r H9C1H10(42) + ρ_r H16C6H17(19) + ρ_w C4H11 (19)
ν_{38}	864	855	825(w)	823		ρ_r H13C5H14(15) + ρ_w C4H11(56)
ν_{39}	614	612	602(w)	602		ρ_r C1-3H (34) + γ C2(46)
ν_{40}	413	416				butterfly(100)
ν_{41}	193	202	197(w)			γ C4H11(72)
ν_{42}	157	167				δ C1-3H(82)
ν_{43}	120	131				δ C5-3H (65)
ν_{44}	106	117				δ C6-3H(65)
ν_{45}	67	79				ρ_t C4C3C6 (48) + ρ_t O7C1C2(52)

Vs, very strong; s, strong; m, middle; w, weak; vw, very weak; ν, stretching; sym, symmetry; asym, asymmetry; δ, in-plane bending; γ, out-of-plane bending; ρ_w, wagging; ρ_r, rocking; ρ_t, twisting; τ, torsion; Ring deforma, ring deformation; PED, potential energy distribution; only contributions larger than 10% were given.

The 239.5 nm resonance Raman frequencies are also included for comparison.

[a]B3LYP/6−31 + G(d) calculated;

[b]scaled = 13.954 + 0.9738 × calculated;

[c]data from 239.5 nm resonance Raman spectrum in cyclohexane solvent.

and thus are respectively assigned as ν_{20}–ν_{17}, whereas the band at 1076 correlates to the calculated one at 1065 cm^{-1}, and is assigned as ν_{35}(A″). In 1300–1500 cm^{-1} region, a broad experimental Raman band at 1444 cm^{-1} correlates with the calculated one at 1487 cm^{-1} (ν_{10}), whereas the four experimental bands at 1340, 1361, 1381, and 1392 cm^{-1} bands correlate with the

calculated ones at 1370, 1390, 1413, and 1423 cm^{-1} (ν_{16}, ν_{15}, ν_{14} and ν_{13}). The well-separated experimental bands at 1645 and 1666 cm^{-1} are respectively assigned as ν_9 and ν_8. The experimental and B3LYP/6-31+G(d) computed vibrational wavenumbers and their tentative assignments are listed in Table 2.

Resonance Raman spectra and excited state structural dynamics

The overall view of the A-band resonance Raman spectra of 3M3P2O in cyclohexane, acetonitrile, and methanol at five laser excitations are shown in Fig. 2. Figure S2 (Supporting Information) displays the expanded view of the 239.5 nm resonance Raman spectra in cyclohexane, acetonitrile, and methanol with the tentative vibrational assignments to larger Raman band features indicated. The weak red-shift of ν_8 is observed when solvent changes from cyclohexane to acetonitrile and to methanol. Figure 3 shows the expanded view of the 223.1 nm resonance Raman spectrum of 3M3P2O in 0–7000 cm^{-1} spectral region in cyclohexane and displays interesting band intensity variations. Most of the A-band resonance Raman intensity can be assigned to the fundamentals, overtones, and combination bands of eight modes: ν_8, ν_9, ν_{10}, ν_{16}, ν_{18}, ν_{19}, ν_{21}, and ν_{25}. The ν_8, ν_9, and their overtones and combination bands with other modes dominate the A-band resonance Raman spectra.

It is well known that the molecular polarizability, which is described by the Kramer-Heisenberg-Dirac (KHD) expression, determines the intensity of Raman scattering of a molecule.[19,20] In the Born-Oppenheimer approximations, the KHD expression can be solved resulting in two terms, known as the Albrecht A-term and B-term.[19,20] The A-term vanishes in the conventional off-resonance RS and only the B-term plays a role. It has a nonzero value only when there is one quantum of vibrational energy difference between the initial and the final states. In other words, unless special effects play a role, overtones and combination bands are extremely weak or not observed in off-resonance RS.

The A-term begins to play an important role in the resonance Raman scattering (including pre-resonance one) if there is a significant difference in the nuclear geometry between the ground and the excited electronic states involved in resonance. In this case, overtones and combination bands through A-term enhancement are strong and will reach maximum at full resonance with the vibronic band.[19–35] For example, the A-band resonance Raman spectra of methyl iodide[25–29] are dominated by the very intense overtones progression of $n\nu_{C-I}$ because of the C—I bond breaking in the excited state. Another example comes from pyrene and anthracene,[34] whose resonance Raman spectra are wavelength dependent and display very strong overtones and combination bands when the laser excitation overlaps with the vibronic band. Figures 2, S2, and 3 show that as the laser excitations go from 252.7 nm to 223.1 nm, the intensities of overtones and combination bands relative to the those of fundamentals increase greatly. This is because 252.7 nm and 223.1 nm are respectively in pre-resonance and in full resonance with the A-band absorption. The significant overtones and combination bands of ν_8 and ν_9 are apparently the vibronic feature of the A-band absorption. Therefore, strong overtones ($n\nu_9$) and combination bands ($n\nu_9 + m\nu_8$) in the A-band resonance Raman spectra of 3M3P2O indicates great C$_3$=C$_4$ and C$_2$=O$_7$ bond length changes in the S$_2$($\pi\pi^*$) state.

The very strong $n\nu_9$ overtone progression of 3M3P2O consists with the electronic nature of the $\pi_{H-1} \rightarrow \pi_L^*$ transition that weakens the C=C bond greatly, as is indicated by the molecular orbitals 26 and 28 in Table 1, and suggests that the S$_2$($\pi\pi^*$) PES along the C=C reaction coordinates possesses the largest slope in FC,[21–24] leading to a great bond order change to form the single-bond like C$_3$—C$_4$ bond in the S$_2$($\pi\pi^*$) state. This is analogue
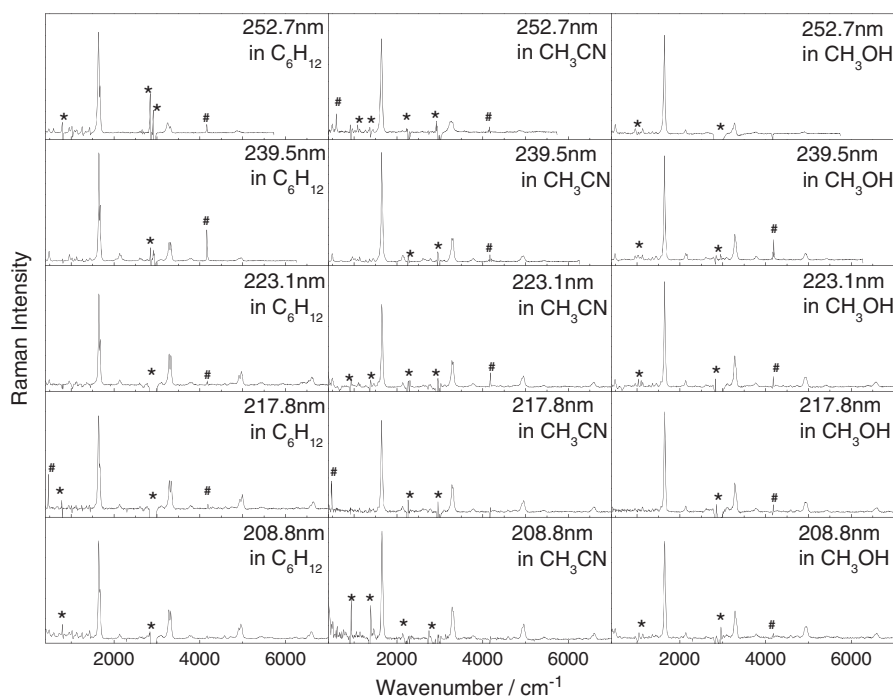

Figure 2. Overview of the 223.1, 217.8, and 208.8 nm resonance Raman spectra of 3M3P2O in cyclohexane, acetonitrile and methanol. Asterisks (*) label the solvent subtraction artifacts. Pounds (#) mark residual uncertain laser lines.
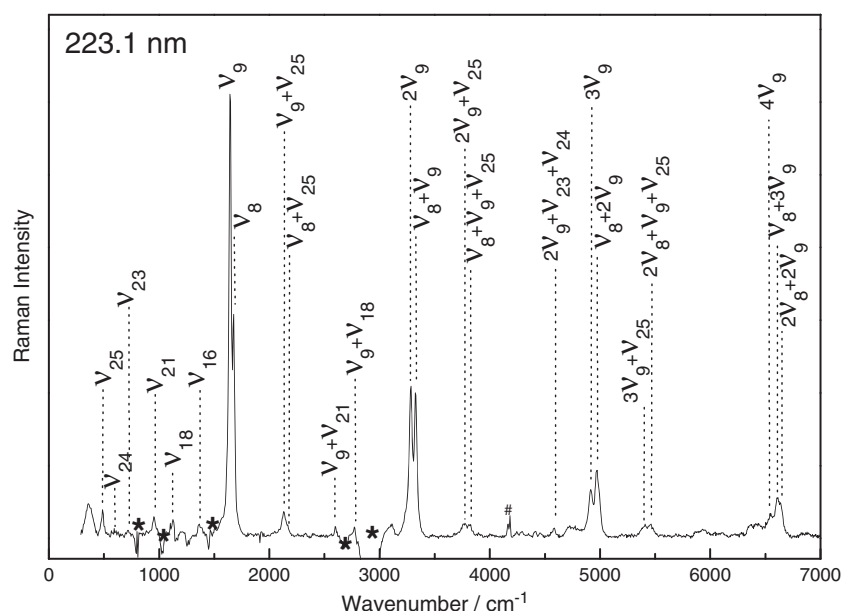
Figure 3. Expanded view of the 223.1 nm resonance Raman spectrum of 3M3P2O in cyclohexane. Pounds (#) mark residual uncertain laser lines.

to the intense overtone progression of C—I stretch fundamental mode of iodomethane, where iodomethane undergoes a direct C—I bond breaking because of $n_I \rightarrow \sigma_{C—I}$ transition.[25–29] Similarly, the very strong combination band progression ($nv_9 + mv_8$) of 3M3P2O suggests that the $C_2=O_7$ double bond of 3M3P2O also undergoes bond order change in so far as the degree of the intensity of a FC active stretch mode correlates the degree of the bond length change in the repulsive PES. In order to speculate the possible intermediate structures such as $S_{2,min}$ ($\pi\pi^*$), the conical intersection point between $S_2(\pi\pi^*)$ and S_1 ($n\pi^*$), we recall the CT-band resonance Raman spectra of the benzene-I_2 and olefin-I_2 complexes,[30–33] where the displayed intensity pattern is to some extent similar to that of the A-band resonance Raman spectra of 3M3P2O. The resonance Raman spectra of the I_2:olefine complexes are dominated by the overtones ($nv_{C=C}$ and $mv_{I—I}$) and combination bands ($nv_{C=C} + mv_{I—I}$) of the I—I and C=C stretch modes, which indicate a simultaneous large bond order changes in the I—I and C=C bonds, and the formation of I—C bond as well as the dissociation of C=C and I—I bonds. Thus, we expect that 3M3P2O in the S_2 ($\pi\pi^*$) state will undergo the large bond elongation of the $C_3=C_4$ and $C_2=O_7$ bonds, and the shortening of the $C_2—C_3$ bond as the molecule moves towards the intermediate states.

Table 3 lists the relative resonance Raman intensities of these bands. Figure 3 and Table 3 show that the band intensity of the $C_3=C_4$ stretch fundamental mode (v_9) is 3.5 times stronger than that of the $C_2=O_7$ stretch fundamental mode (v_8), whereas the band intensity of the overtone $2v_9$ is in intensity comparable with its combination band $v_9 + v_8$ (about 1.2 : 1.0). The band intensity of the third overtone $3v_9$ or forth overtone $4v_9$ becomes respectively further weaker (1.0 : 1.8 or 1.0 : 2.1) relative to the combination band $2v_9 + v_8$ or $3v_9 + v_8$. In short, the overtone progression nv_9 vanish at about $4v_9$, whereas the combination bands $3v_9 + v_8$ still has significant intensity. That is to say the combination bands maintain intensity while the overtones are diminished. This suggests that when the wave-packet evolves on the $S_2(\pi\pi^*)$ PES, the propagating wave-packet evolves initially along the major ethylenic stretch coordinate and the moderate carbonyl

Table 3. Relative Raman intensities of fundamentals, overtones and combination bands of the 223.1 nm resonance Raman spectra of 3M3P2O in cyclohexane. Δ_9 and Δ_8 are estimated using the intensities of the fundamentals modes v_9 and v_8, while Δ_9' and Δ_8' are estimated using the intensities of the $4v_9$ and $2v_9 + 2v_8$

mode	Rel. Int.	Intensity ratio	Δ_i
v_9	100	3.5 : 1.0	$\Delta_9 = 1.00$
v_8	28.5		$\Delta_8 = 0.52$
$2v_9$	39.0	1.2 : 1.0	
$v_9 + v_8$	32.2		
$3v_9$	14.8	1.0 : 1.8	
$2v_9 + v_8$	26.1		
$4v_9$	6.3	$4v_9 : 3v_9 + v_8 = 1.0 : 2.1$	$\Delta_9' = 1.00$
$3v_9 + v_8$	13.3		
$2v_9 + 2v_8$	7.0	$4v_9 : 2v_9 + 2v_8 = 1.0 : 1.1$	$\Delta_8' \cong 1.03$

stretch coordinate, followed by along the major carbonyl and ethylenic stretch coordinates at longer evolution time.

The resonance Raman intensity pattern of a molecule can be well modeled by the time-dependent wave-packet theory in simple model if the interested excited state is a single, nondegenerate excited state.[21–24] In this case, the only feature of relevance to the Raman scattering process is the slope of the excited electronic state PES at the geometry of the minimum of the ground state surface if the UV absorption spectral line broadening is due to rapid dephasing (called the short time approximation). Alternatively, the standard Kramers-Heisenberg-Dirac treatment of Raman scattering in the Condon or A-term approximation results in intensities for the fundamental transition of mode i proportional to $\Delta_i^2 \omega_i^2$, where the normal mode displacement Δ_i and the frequency ω_i refer to the i-th normal mode. The relative intensity of two modes i and j is independent of excitation wavenumber. In literature, it has well been established that the greater the Δ_i value of a certain vibrational mode, the longer the overtone progression of the mode if simple model

holds. This has been proved to be true by many tested molecular systems like iodine,[20] methyl iodide,[25–29] benzene-I_2 complex,[30] and olefine-I_2 complexes,[31–33] and CH_3NO_2,[35] whose intensity patterns were well modeled by the time-dependent wave-packet theory in simple model and in short-time limit.

Hudson and coworker developed an ab initio method to calculate relative resonance Raman intensities of the fundamental vibrational modes for molecular systems that meet the simple model.[36] They noted that in the short time limit, the relative Raman intensities of fundamentals do not depend on the excitation wavelength and the electronic origin for the resonant transition is no longer a relevant parameter. The electronic origin and the transition oscillator strength are important for describing the absolute intensity or the relative intensity of two spectra at different excitation wavelengths but are not needed if the objective is to calculate the relative intensity of the various enhanced vibrational transitions. This method is adopted in present work to estimate the normal mode displacements Δ_i evaluated at the FC point, and the calculated results together with the comparison to the experimental ones are listed in Table 4 for 3M3P2O. It shows that the B3LYP-TD/6−31++G(d,p) predicted relative band intensities of the fundamental modes v_8, v_9, v_{10}, v_{16}, v_{18}, v_{19}, v_{21}, v_{24}, v_{25}, and v_{26} reproduce well with the corresponding band intensities of the fundamentals in the 223.1 nm resonance Raman spectra in three solvents. It appears that the time-dependent density functional theory in short-time limit works well in predicting the initial slopes of the $S_2(\pi\pi^*)$ PES that govern the intensities of the fundamentals.

The B3LYP-TD/6−31++G(d,p) calculated relative normal mode displacements (Δ_i) for v_9 and v_8 are, respectively, 1.00 (taken as relative standard) and 0.585, as shown in Table 3 and this indicates that the initial slope of the excited state PES along the C=C reaction coordinate is much steeper than that along C=O reaction coordinate. Because in short-time limit those modes that have steepest slope or undergo the largest excited state geometry changes will exhibit the highest fundamental intensities and the longest overtone progressions if the two slopes keep

unchanged when the wave-packets evolve on the pure $S_2(\pi\pi^*)$ state, we thus expect that the C=C stretch mode v_9 will have longest overtone progressions, or in other words that for n equals m the intensity of nv_9 will be more intense than that of mv_8 or $(n-1)v_9 + v_8$. This is apparently not in a good agreement with experimental observation that the intensities of $2v_9 + v_8$ and $3v_9 + v_8$ are actually greater than those of $3v_9$ and $4v_9$, respectively.

The possible argument is that the slopes or the normal mode displacements of 3M3P2O vary as the wave-packet evolves. This can be verified either quantitatively or qualitatively. Previous practices indicate that the quantitative determination of $|\Delta_i|$ require simultaneous fitting of the experimental absorption cross section and the absolute Raman cross sections and use a set of intensity standards each time (basically, they can be the fundamentals or the overtones and/or combination bands), and this needs future effort. Therefore, for easy specification, the equation $I_i = \Delta_i^2 \omega_i^2$ is used to qualitatively determine $|\Delta_i|$ and the results for the estimated relative $|\Delta_9|$ and $|\Delta_8|$ are listed in Table 3. It shows that $|\Delta_9|$ and $|\Delta_8|$ are respectively 1.00 and 0.52 if v_9 and v_8 fundamentals are used as the intensity standards, which is in a good agreement with 1.00 and 0.585 estimated by the B3LYP-TD/6−31++G(d,p) computation in Table 4. Table 3 also shows that $|\Delta_9'|$ and $|\Delta_8'|$ are, respectively, 1.00 and 1.03 when $4v_9$ and $2v_9 + 2v_8$ are used as the intensity standards (Table 3).

The slope of the $S_2(\pi\pi^*)$ excited state PES along the C=O reaction coordinate appears to vary. The non-Condon mechanism would be one possible explanation because the variation of the vibrational force constants or Duschinsky effect during the wave-packet motion in the excited state are apparently time-dependent in nature.[37] An alternative explanation is that at the very beginning, the $\pi \rightarrow \pi^*$ vertical electronic transition causes the electronic density varies mainly on the C=C moiety so that larger slope along v_9 than along v_8 reaction coordinate is expected in the initial wave-packet motion, just as the B3LYP-TD/6−31++G(d,p) predicted normal mode displacement $|\Delta_9|$ is much larger than $|\Delta_8|$, whereas at longer evolution time when the C=C bond undergoes significant bond length elongation, the charge-redistribution occurs continuously in the C=C—C=O moiety and the structural reorganization required by the $S_2(\pi\pi^*)/S_1(n\pi^*)$ conical intersection point makes the slope along $C_2=O_7$ reaction coordinate become comparable or even greater than that along the $C_3=C_4$ reaction coordinate (for details, see the section on Excited State Structures, Conical Intersections and Decay Dynamics).

Excited state structures, conical intersections and decay dynamics

In order to explore the excited state reaction dynamics, curve-crossing points of 3M3P2O, and the effect of the $S_2(\pi\pi^*)/S_1(n\pi^*)$ conical intersection point on the A-band resonance Raman intensity pattern, we have carried out the CASSCF calculation to determine the vertical electronic transition energies and the optimized excited state geometries as well as the geometry structures of the conical intersection points. Table 4 lists the CASSCF(6,5)/6−31G(d) calculated minimal singlet excitation energies of $S_{1,FC}$, $S_{1,min}$ $(n\pi^*)$, $S_{2,FC}$, $S_{2,min}$ $(\pi\pi^*)$, and the transition energies of the conical intersection points S_n/S_π and S_n/S_0. The optimized geometry structures are presented in Fig. 4 and the corresponding structural parameters are listed in Table S1 (Supporting Information). Figure 4 and Table S1 (Supporting Information) show that the molecular symmetry for optimized

Table 4. B3LYP-TD/6−31++G(d,p) calculated normal mode displacements $|\Delta_i|$ and relative A-band resonance Raman intensities of the fundamental vibrational modes, and their comparison to the experimental ones

Modes	Freq. /cm^{-1} [a]	Relative intensity Expt. [a]	Relative intensity Calc.	Normal mode displacement $|\Delta_i|$ Calc.
v_8	1678	0.35	0.34	0.585
v_9	1643	1.00	1.00	1.000
v_{10}	1436	0.07	0.03	0.156
v_{16}	1360	0.01	0.01	0.013
v_{18}	1130	0.04	0.03	0.133
v_{19}	1083	0.02	0.00	0.011
v_{21}	954	0.09	0.00	0.034
v_{24}	593	0.00	0.00	0.021
v_{25}	487	0.13	0.09	0.157
v_{26}	407	0.01	0.01	0.035

[a]: data from 239.5 nm resonance Raman spectrum in cyclohexane solvent;
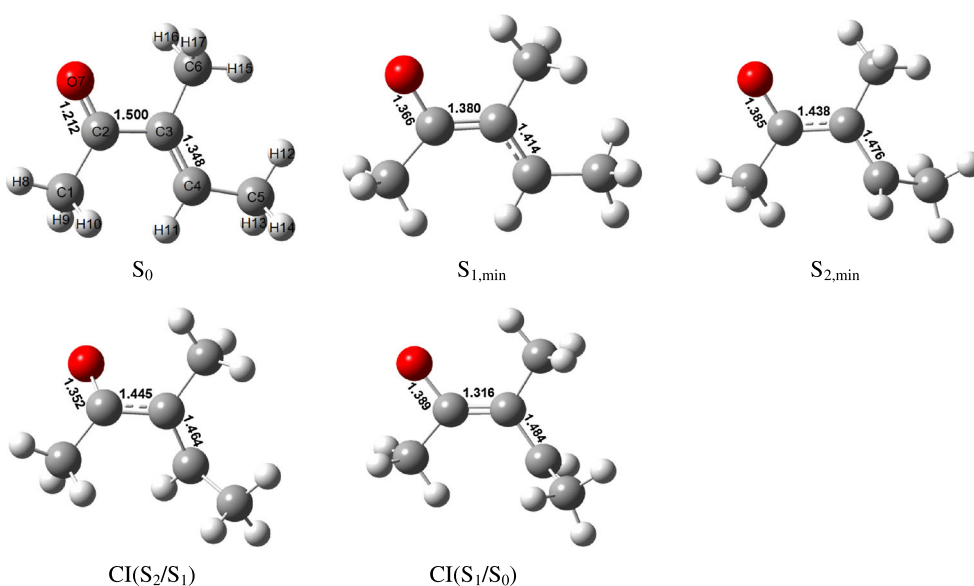[b]: B3LYP-TD/6−31++G(d, p) calculated.

Figure 4. The optimized geometry structures and the structural parameters for $S_{1,min}$ ($n\pi^*$), $S_{2,min}$ ($\pi\pi^*$) and the conical intersection points $S_1(n\pi^*)/S_2$ ($\pi\pi^*$) and $S_n(n\pi^*)/S_0$.

geometry structures of 3M3P2O in singlet and triplet excited states as well as curve-crossing points are all in C_1 point group.

The second lowest lying singlet excited state is the light-absorbing $S_2(\pi\pi^*)$ state. The largest bond length changes at the $S_{2,min}(\pi\pi^*)$ structure occur at the $C_2=O_7$, $C_3=C_4$ and C_2—C_3 bonds relative to those in ground state. The $C_2=O_7$ and $C_3=C_4$ bond lengths elongate to 1.385 Å and 1.476 Å and they are longer than those in the ground state by 0.173 Å and 0.128 Å, whereas C_2—C_3 bond length shortens to 1.438 Å and it is shorter than that in ground state by 0.062 Å. The degree of the $C_2=O_7$ bond length change (+0.173 Å) is greater than that of the $C_3=C_4$ bond length change (+0.128 Å). The lowest lying singlet excited state at the optimized ground-state geometry is the $S_1(n\pi^*)$ state. The largest bond length changes occur at the $C_2=O_7$, $C_3=C_4$, and C_2—C_3 bonds. The $C_2=O_7$ and $C_3=C_4$ bond lengths elongate to 1.366 Å and 1.414 Å, which are longer than those in the ground state by 0.154 and 0.066 Å, whereas C_2—C_3 bond length shortens to 1.380 Å, shorter than that in ground state by 0.12 Å.

The minimal excitation energies for $S_{1,min}(n\pi^*)$ and $S_{2,min}(\pi\pi^*)$ and $S_2(\pi\pi^*)/S_1(n\pi^*)$ and $S_1(n\pi^*)/S_0$ are, respectively, 56, 118.8, 107.8 and 67.3 kcal/mol. Because the A-band absorption is broad and structureless, which is indicative of a very short lifetime of the $S_2(\pi\pi^*)$ state,[15] and because the laser excitations that cover the A-band absorption do not produce any fluorescence for the resonance Raman scatterings, the major decay channel is that the molecule transits to the $S_1(n\pi^*)$ state via $S_2(\pi\pi^*)/S_1(n\pi^*)$ internal conversion but not down to the $S_{2,min}(\pi\pi^*)$ structure emits fluorescence. Thus, the role of the $S_{2,min}(\pi\pi^*)$ in decay processes is ignored and the correlation between the $S_{2,min}(\pi\pi^*)$ structure and the A-band resonance Raman intensity is abandoned.

Resonance Raman spectroscopy has been applied to probe the conical intersectional dynamics (~80 fs) of thiophene,[38] 4-cyanobenzaldehyde,[39] pyrazine,[40], and so on. Our results demonstrate that there are good correlations between the initial short-time structural dynamics and the structures of the conical intersections. The timescale revealed by femtosecond time-resolved photoelectron spectroscopy for the $S_2(\pi\pi^*)$/ $S_1(n\pi^*)$ conical intersectional dynamics of α,β-enones is about 60–90 fs.[15] This suggests the ultrafast decay dynamics

switching from $S_2(\pi\pi^*)$ to $S_1(n\pi^*)$ for 3M3P2O is in timescale detectable by the resonance Raman spectroscopy. Thus, the use of the $S_2(\pi\pi^*)/S_1(n\pi^*)$ structure to correlate to the A-band resonance Raman intensity pattern is feasible.

The largest bond length changes of the $S_2(\pi\pi^*)/S_1(n\pi^*)$ structure occur at the $C_2=O_7$, $C_3=C_4$, and C_2—C_3 bonds relative to those in ground state. The $C_2=O_7$ and $C_3=C_4$ bond lengths elongate to 1.352 Å and 1.464 Å and they are longer than those in the ground state by 0.14 Å and 0.116 Å. The great $C_2=O_7$ and $C_3=C_4$ bond length changes in the $S_2(\pi\pi^*)/S_1(n\pi^*)$ structure agree qualitatively with the intensity patterns of the long overtone progression of $n\nu_9$ and the ever longer combination band progression of $\nu_9 + \nu_8$, $2\nu_9 + \nu_8$, $3\nu_9 + \nu_8$, $2\nu_9 + 2\nu_8$, $3\nu_9 + 2\nu_8$, as shown in Fig. 3, and this consistently indicates that the structural dynamics of 3M3P2O at longer evolution time (required to reach conical intersection point) is towards more $C_2=O_7$ double bond elongation relative to the $C_3=C_4$ bond length lengthening, or the degree of the $C_2=O_7$ and $C_3=C_4$ bond lengthening evaluated at FC is apparently different than that at longer evolution time towards to the $S_2(\pi\pi^*)/S_1(n\pi^*)$ point. That the $C_3=C_4$ bond length lengthens greater at the very beginning, whereas the $C_2=O_7$ bond length lengthens greater at the later evolution time is also in a good agreement with the variation of the state mixing between the $S_2(\pi\pi^*)$ and the $S_1(n\pi^*)$ states, which, featured by the coefficients of the orbital transitions, varies from 0.69/0.1 for $\pi_{H-1} \rightarrow \pi^*_L/n_H \rightarrow \pi_L^*$ transitions at FC point, to 0.5/0.5 for $\pi_{H-1} \rightarrow \pi^*_L/n_H \rightarrow \pi_L^*$ transitions at $S_2(\pi\pi^*)/S_1(n\pi^*)$ point.

The decay dynamics in singlet realm is proposed as follows: as the wave-packet evolves from FC point, the initial structural change is predominantly along C=C reaction coordinate, followed by an increasing change along C=O reaction coordinate. Upon the wave-packet leaves away from the FC point, 3M3P2O reorganizes its structure through the bend-out of O_7 atom, the rotation of the C_5/C_6 methyl groups, and the great bond length elongation of the C=C and C=O bond to finally reach to the $S_2(\pi\pi^*)/S_1(n\pi^*)$ conical intersection point, where the molecules switch to the S_1 ($n\pi^*$) state to finally intersects the ground state or the low-lying triplet states. Figure 5 shows the schematic diagram of the decay dynamics of 3M3P2O from $S_2(^1\pi\pi^*)$ to $S_1(^1\pi\pi^*)$ via $S_2(\pi\pi^*)/S_1(n\pi^*)$
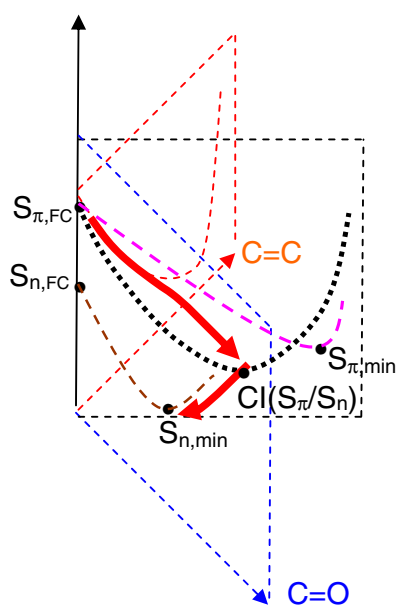
Figure 5. Schematic diagram of the decay dynamics of 3M3P2O from S_2 ($^1\pi\pi^*$) to S_1($^1\pi\pi^*$) via $S_2(\pi\pi^*)/S_1(n\pi^*)$.

in singlet realm. The red solid line shows that at the very beginning, the wave-packet evolves along the major C=C stretch coordinate for some distance first, and then more and more along the C=O stretch coordinate in addition to the major C=C stretch coordinate until the molecule reaches to the $S_2(\pi\pi^*)/S_1$ ($n\pi^*$) point. The decay dynamics in triplet realm are also studied on the basis of the CASSCF calculation, and the results are included Table S2 (Supporting Information), Figs. S3 and S4 (Supporting Information).

Conclusion

The photophysics of 3M3P2O after excitation to $S_2(\pi\pi^*)$ electronic state were studied using the resonance Raman spectroscopy and CASSCF method calculations. The intense A-band absorption is assigned as $\pi_{H-1} \rightarrow \pi_L^*$ transition. Most of the A-band resonance Raman intensity can be assigned to the fundamentals, overtones and combination bands of eight modes: ν_8, ν_9, ν_{10}, ν_{16}, ν_{18}, ν_{19}, ν_{21}, and ν_{25}. The B3LYP-TD/6−31++G(d, p) predicted relative Raman band intensities of the fundamental modes ν_8, ν_9, ν_{10}, ν_{16}, ν_{18}, ν_{19}, ν_{21}, ν_{24}, ν_{25}, and ν_{26} reproduce well with the corresponding fundamental band intensities of the 223.1 nm resonance Raman spectrum. It reveals that the initial structural dynamics are predominantly along the $S_2(\pi\pi^*)$ PES, and the largest structural changes appear in the motions along the $C_3=C_4$ stretch (ν_9) and the $C_2=O_7$ stretch (ν_8) reaction coordinates.

The band intensity of the $C_3=C_4$ stretch fundamental mode (ν_9) is 3.5 times stronger than that of the $C_2=O_7$ stretch fundamental mode (ν_8), whereas the band intensity of the third overtone $3\nu_9$ or forth overtone $4\nu_9$ becomes much weaker (1.0 : 1.8 or 1.0 : 2.1) than the combination band $2\nu_9 + \nu_8$ or $3\nu_9 + \nu_8$. In short, the overtone progression $n\nu_9$ vanish at about $4\nu_9$, whereas the combination bands $3\nu_9 + \nu_8$ still has significant intensity. Such resonance Raman intensity pattern is hardly explained by the relative normal mode displacements ($\Delta_9 = 1.000$ and $\Delta_8 = 0.585$) predicted by B3LYP-TD/6−31++G(d,p) calculation if Δ_i keep constant during the wave-packet motion in the excited state PES.

The argument is that the slopes or the normal mode displacements of 3M3P2O vary as the wave-packet evolves in the excited state PES. This is qualitatively verified by the fact that $|\Delta_9|$ and $|\Delta_8|$ determined by equation $I_i = \Delta_i^2 \omega_i^2$ for ν_9 and ν_8 vary greatly when ν_9/ν_8, and $4\nu_9/2\nu_9 + 2\nu_8$ are respectively selected as the intensity standard. The argument is also supported by the major bond length changes of the $S_2(\pi\pi^*)/S_1(n\pi^*)$ structure relative to S_0. The great $C_2=O_7$ and $C_3=C_4$ bond length changes in the S_2 ($\pi\pi^*$)/$S_1(n\pi^*)$ structure agree qualitatively with the intensity patterns of the long overtone progression of $n\nu_9$ and the ever longer combination band progression of $\nu_9 + \nu_8$, $2\nu_9 + \nu_8$, $3\nu_9 + \nu_8$, $2\nu_9 + 2\nu_8$, $3\nu_9 + 2\nu_8$, and this consistently indicates that the structural dynamics of 3M3P2O at longer evolution time towards the $S_2(\pi\pi^*)/S_1(n\pi^*)$ point is more along the $C_2=O_7$ bond elongation than along the $C_3=C_4$ bond lengthening as comparison to that in FC.

The transition energies of the conical intersection/intersystem crossing points S_n/S_π, S_n/S_0, T_1/T_2, T_2/T_3, S_0/T_1, S_1/T_1, S_1/T_2, S_2/T_3 are, respectively, predicted at the CASSCF(6,5)/6−31G(d) level of theory. A three state intersystem crossing point $ISC(S_1/T_2/T_1)$ is found to be in energy a bit higher than that of $S_{1,min}(n\pi^*)$. The decay dynamics of 3M3P2O from $S_2(^1\pi\pi^*)$ to $S_1(^1\pi\pi^*)$ via S_2 ($\pi\pi^*$)/$S_1(n\pi^*)$ in singlet realm and from $S_1(n\pi^*)$ to $T_1(n\pi^*)$ via ISC $[S_1(n\pi^*)/T_2(\pi\pi^*)/T_1(n\pi^*)]$ in triplet realm are proposed:
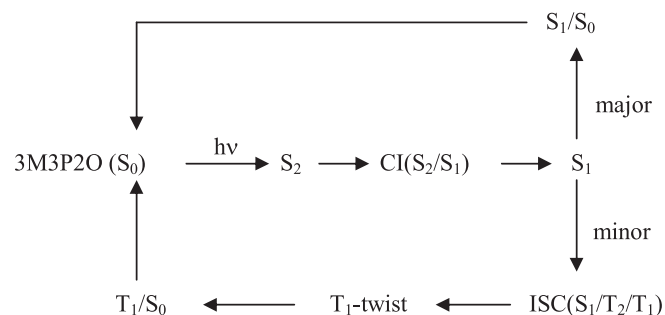
Reference

[1] A. D. Walsh, *Trans. Faraday Soc.* **1945**, *41*, 498.
[2] R. S. Becker, K. Inuzuka, J. King, *J. Chem. Phys.* **1970**, *52*, 5164.
[3] J. W. Coomber, J. N. Pitts, *J. Am. Chem. Soc.* **1969**, *91*, 547.
[4] H. Shinohara, N. Nishi, *J. Chem. Phys.* **1982**, *77*, 234.
[5] M. E. Umstead, R. G. Shortridge, M. C. Lin, *J. Phys. Chem.* **1978**, *82*, 1455.
[6] G. T. Fujimoto, M. E. Umstead, M. C. Lin, *J. Chem. Phys.* **1985**, *82*, 3042.
[7] B. M. Haas, T. K. Minton, P. Felder, J. R. Huber, *J. Phys. Chem.* **1991**, *95*, 5149.
[8] M. F. Arendt, P. W. Browning, L. J. Butler, *J. Chem. Phys.* **1995**, *103*, 5877.
[9] R. Bonneau, *J. Am. Chem. Soc.* **1980**, *102*, 3816.
[10] D. I. Schuster, D. A. Dunn, G. E. Heibel, P. B. Brown, J. M. Rao, J. Woning, R. Bonneau, *J. Am. Chem. Soc.* **1991**, *113*, 6245.
[11] R. Bonneau, Ph. Fornier de Violet, *CR Acad. Sci., Ser. C* **1977**, *284*, 631.
[12] M. Reguero, M. Olivucci, F. Bernardi, M. A. Robb, *J. Am. Chem. Soc.* **1994**, *116*, 2103.
[13] W.-H. Fang, *J. Am. Chem. Soc.* **1999**, *121*, 8376.

Journal of RAMAN SPECTROSCOPY

[14] E. G. Expósito, M. J. Bearpark, R. M. Ortuño, V. Branchadell, M. A. Robb, and S. Wilsey, *J. Org. Chem.* **2001**, *66*, 8811.

[15] A. M. D. Lee, J. D. Coe, S. Ullrich, M.-L. Ho, S.-J. Lee, B.-M. Cheng, M. Z. Zgierski, I.-C. Chen, T. J. Martinez, A. Stolow, *J. Phys. Chem. A* **2007**, *111*, 11948.

[16] X. M. Zhu, S. Q. Zhang, X. M. Zheng, D. L. Phillips, *J. Phys. Chem. A* **2005**, *109*, 3086.

[17] K. F. Weng, Y. Shi, X. M. Zheng, D. L. Phillips, *J. Phys. Chem. A* **2006**, *110*, 851.

[18] M. J. Frisch, G. W. Trucks, H. B. Schlegel, G. E. Scuseria, M. A. Robb, J. R. Cheeseman, G. Scalmani, V. Barone, B. Mennucci, G. A. Petersson, H. Nakatsuji, M. Caricato, X. Li, H. P. Hratchian, A. F. Izmaylov, J. Bloino, G. Zheng, J. L. Sonnenberg, M. Hada, M. Ehara, K. Toyota, R. Fukuda, J. Hasegawa, M. Ishida, T. Nakajima, Y. Honda, O. Kitao, H. Nakai, T.Vreven, J. A. Montgomery, J. E. Peralta, F. Ogliaro, M. Bearpark, J. J. Heyd, E. Brothers, K. N. Kudin,V. N. Staroverov, R. Kobayashi, J. Normand, K. Raghavachari, A. Rendell, J. C. Burant, S. S. Iyengar, J. Tomasi, M. Cossi, N. Rega, J. M. Millam, M. Klene, J. E. Knox, J. B. Cross, V. Bakken, C. Adamo, J. Jaramillo, R. Gomperts, R. E. Stratmann, O. Yazyev, A. J. Austin, R. Cammi, C. Pomelli, J. W. Ochterski, R. L. Martin, K. Morokuma, V. G. Zakrzewski, G. A. Voth, P. Salvador, J. J. Dannenberg, S. Dapprich, A. D. Daniels, O. Farkas, J. B. Foresman, J. V. Ortiz, J. Cioslowski, D. J. Fox, Gaussian 09, Revision .A.1, Gaussian, Inc., Wallingford CT, **2009**.

[19] J. L. McHale, Molecular Spectroscopy, Prentice Hall, Upper Saddle River, NJ, **1999**, Chapter 12.

[20] W. E. Smith, G. Dent, Modern Raman Spectroscopy, Wiley and Sons, London, **2005**, Chapter 4.

[21] S.-Y. Lee, E. J. Heller, *J. Chem. Phys.* **1979**, *71*, 4777.

[22] E. J. Heller, R. L. Sundberg, D. Tannor, *J. Phys. Chem.* **1982**, *86*, 1822.

[23] A. B. Myers, R. A. Mathies, in Biological Applications of Raman Spectroscopy (Ed.: T. G. Spiro), Wiley, New York, **1987**, p 2.

[24] A. B. Myers, in Laser Techniques in Chemistry (Eds.: A. B. Myers, T. R. Rizzo), Wiley, New York, **1995**, p 325.

[25] D. Imre, J. L. Kinsey, A. Sinha, J. Krenos, *J. Phys. Chem.* **1984**, *88*, 3956.

[26] G. E. Galica, B. R. Johnson, J. L. Kinsey, M. O. Hale, *J. Phys. Chem.* **1991**, *95*, 7994.

[27] K. O. Lao, M. D. Person, P. Xayariboun, L. J. Butler, *J. Chem. Phys.* **1990**, *92*, 823.

[28] F. Markel, A. B. Myers, *J. Chem. Phys.* **1993**, *98*, 21.

[29] P. G. Wang, L. D. Zeigler, *J. Phys. Chem.* **1993**, *97*, 3139.

[30] K.-F. Weng, Y. Shi, X. Zheng, D. L. Phillips, *J. Phys. Chem. A* **2006**, *110*, 851.

[31] X. Zheng, W. H. Fang, D. L. Phillips, *Chem. Phys. Lett.* **2001**, *342*, 425.

[32] S. P. Li, G. M. Wu, X. Zheng, *Chem. J. Chinese Universities* **2004**, *25*, 1495.

[33] H. F. Zhu, X. Zheng, *Chem. J. Chinese Universities* **2005**, *26*, 1921.

[34] E. V. Efremov, F. Ariese, A. J. G. Mank, C. Gooijer, *Anal. Chem.* **2006**, *78*, 3152.

[35] D. L. Phillips, A. B. Myers, *J. Phys. Chem.* **1991**, *95*, 7164.

[36] B. S. Hudson, L. M. Markham, *J. Raman Spectrosc.* **1998**, *29*, 489.

[37] B. R. Stallard, P. R. Callis, P. M. Champion, A. C. Albrecht, *J. Chem. Phys.* **1984**, *80*, 70.

[38] X.-F. Wu, X. Zheng, H.-G. Wang, Y.-Y. Zhao, X.-G. Guan, D. L. Phillips, X.-B. Chen, W.-H. Fang, *J. Chem. Phys.* **2010**, *133*, 134507.

[39] Y. Yang, S. Pan, J.-D. Xue, X. Zheng, W.-H. Fang, D. L. Phillips, *J. Raman Spectrosc.* **2014**, *45*, 105.

[40] J.-L. Guo, C. Liu, B.-B. Xie, Y.-Y. Zhao, K.-M. Pei, H.-G. Wang, X. Zheng, *J. Raman Spectrosc.* **2012**, *43*, 1477.

Supporting information

Additional supporting information may be found in the online version of this article at the publisher's web site.

447